Geochemistry Geophysics Geosystems G3
AN ELECTRONIC JOURNAL OF THE EARTH SCIENCES
Published by AGU and the Geochemical Society

Technical Brief
Volume 9, Number 5
28 May 2008
Q05020, doi:10.1029/2008GC001981
ISSN: 1525-2027

Surface wave tomography of China from ambient seismic noise correlation

Sihua Zheng
Institute of Earthquake Science, China Earthquake Administration, No. 63, Fuxing Avenue, Beijing, 100036, China
Department of Geology, University of Illinois, 1301 West Green Street, 245 NHB, Urbana, Illinois 61891, USA

Xinlei Sun and Xiaodong Song
Department of Geology, University of Illinois, 1301 West Green Street, 245 NHB, Urbana, Illinois 61891, USA (xsong@uiuc.edu)

Yingjie Yang and Michael H. Ritzwoller
Department of Physics, University of Colorado at Boulder, Campus Box 390, Boulder, Colorado 80309, USA

[1] We perform ambient noise tomography of China using data from the China National Seismic Network and surrounding global and regional stations. For most of the station pairs, we retrieve good Rayleigh waveforms from ambient noise correlations using 18 months of continuous data at all distance ranges across the entire region (over 5000 km) and for periods from 70 s down to about 8 s. We obtain Rayleigh wave group velocity dispersion measurements using a frequency-time analysis method and invert for Rayleigh wave group velocity maps for periods from 8 s to 60 s. The tomographic maps display significant features that correlate with surface geology. Major basins, including Tarim, Junggar, Qadaim, Sichuan, Bohai-Wan, and Songliao, are all well delineated by slow group velocities at shorter periods (10 to 20 s). The overall trend of crustal thickening from east to west is well represented by group velocity decreases from east to west at periods around 30 s.

Components: 3888 words, 7 figures.

Keywords: surface wave; tomography; ambient noise correlation; China.

Index Terms: 7255 Seismology: Surface waves and free oscillations; 7270 Seismology: Tomography (6982, 8180); 7205 Seismology: Continental crust (1219).

Received 5 February 2008; **Revised** 18 March 2008; **Accepted** 26 March 2008; **Published** 28 May 2008.

Zheng, S., X. Sun, X. Song, Y. Yang, and M. H. Ritzwoller (2008), Surface wave tomography of China from ambient seismic noise correlation, *Geochem. Geophys. Geosyst.*, *9*, Q05020, doi:10.1029/2008GC001981.

1. Introduction

[2] Recent theoretical and laboratory studies have shown that the Green functions of a structure can be obtained from the cross correlation of diffuse wavefields [e.g., *Lobkis and Weaver*, 2001] (see also review by *Campillo* [2006]). The basic idea is that linear waves preserve, regardless of scattering, a residual coherence that can be stacked and amplified to extract coherent information between receivers [e.g., *Weaver*, 2005]. The idea has now found rapid applications in seismology. In particu-

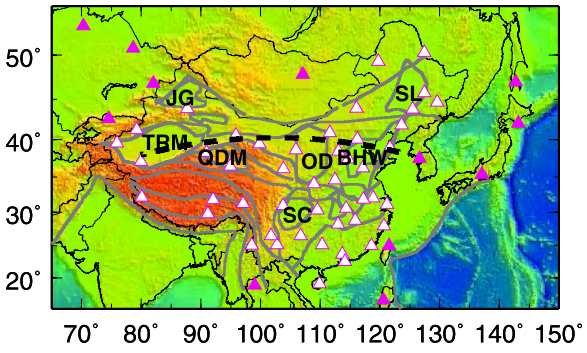

Figure 1. Distribution of seismic stations used in this study, including China National Seismic Network (CNSN) stations (open triangles) and stations in the surrounding regions (solid triangles). Plotted also are major tectonic boundaries [from *Liang et al.*, 2004] and major basins. The basins that are labeled include Tarim (TRM), Junggar (JG), Qaidam (QD), Sichuan (SC), Ordos (OD), Bohai Wan (BHW), and Songliao (SL) basins. The thick dashed line across northern China from the Tarim Basin to Korea indicates the selected great circle path for Figure 6.

lar, surface waves have been found to be most easily retrievable from the cross correlations of seismic coda [*Campillo and Paul*, 2003; *Paul et al.*, 2005] or ambient noise [*Shapiro and Campillo*, 2004; *Shapiro et al.*, 2005; *Sabra et al.*, 2005a, 2005b] between two stations. Both Rayleigh waves and Love waves can be retrieved. The new type of data has rapidly been used for tomographic mapping at regional or local scales [e.g., *Shapiro et al.*, 2005; *Sabra et al.*, 2005b; *Kang and Shin*, 2006; *Villaseñor et al.*, 2007; *Liang and Langston*, 2008] and on continental scales [e.g., *Yang et al.*, 2007; *Bensen et al.*, 2008]. These studies have focused on Rayleigh wave group velocity tomography from ambient noise. However, the method has been demonstrated to be applicable to Love waves [*Lin et al.*, 2008] and phase velocity measurements [*Yao et al.*, 2006; *Lin et al.*, 2008].

[3] Ambient noise tomography (ANT) overcomes several important limitations of conventional methods based on earthquakes, i.e., uneven distribution of earthquake sources, uncertainty in earthquake location, and attenuation of short-period surface waves. Thus, the method is particularly useful for surface-wave path calibration and for tomographic mapping in aseismic regions especially at short periods (below 30 s).

[4] In this study, we applied the ANT techniques to China. Prior surface wave dispersion and inversion studies of the region have relied on a sparse network of the Chinese Digital Seismic Network (CDSN) (with 10 stations) established in 1986 and other global stations in adjacent regions [e.g., *Zhang and Lay*, 1996; *Wu et al.*, 1997; *Ritzwoller and Levshin*, 1998; *Curtis et al.*, 1998; *Xu et al.*, 2000; *Zhu et al.*, 2002; *Huang et al.*, 2003; *Lebedev and Nolet*, 2003; *Yao et al.*, 2005]. The surface wave periods range from about 10 s up to 250 s. Here we obtain inter-station dispersion measurements and perform ANT of China using stations from the new China National Seismic Network (CNSN) and a few stations in the surrounding regions (Figure 1). The CNSN is the national backbone network, established around 2000, with a relatively uniform distribution across the continental China. We focus on Rayleigh wave group velocities in this study. The dispersion measurements and tomographic maps provide a brand new and complementary data set critically needed for constraining the 3-D structure of the region.

2. Data and Method

[5] We use 18 months of continuous data from 47 CNSN stations and 12 other stations. All stations are broadband. The bandwidths of the CNSN stations are from 20 Hz to at least 120 s. We use the data processing and imaging techniques described in detail by *Bensen et al.* [2007]. To avoid the redundancy we summarize our data processing only briefly below.

[6] We first obtain the empirical Green function (EGF) from ambient noise cross correlation. Continuous data are pre-processed before correlation and stacking, which includes clock synchronization, removal of instrument response, time domain filtering, temporal normalization and spectral whitening. The purpose is to reduce the influence of earthquake signals and instrument irregularities and to enhance the strength and bandwidth of the ambient noise correlations. In particular, we follow *Bensen et al.* [2007] and perform time domain normalization, which normalizes the time series by a running average. The running average is computed between 15 and 25 s period, a band in which small earthquakes are typically stronger than microseismic noise. Bensen tested it versus sign bit normalization and found it superior in the presence of numerous small earthquakes within the seismic array. Cross correlations are done daily and then stacked over all time periods (18 months). All the processes are linear, so breaking the cross correlation into daily procedures, rather than performing

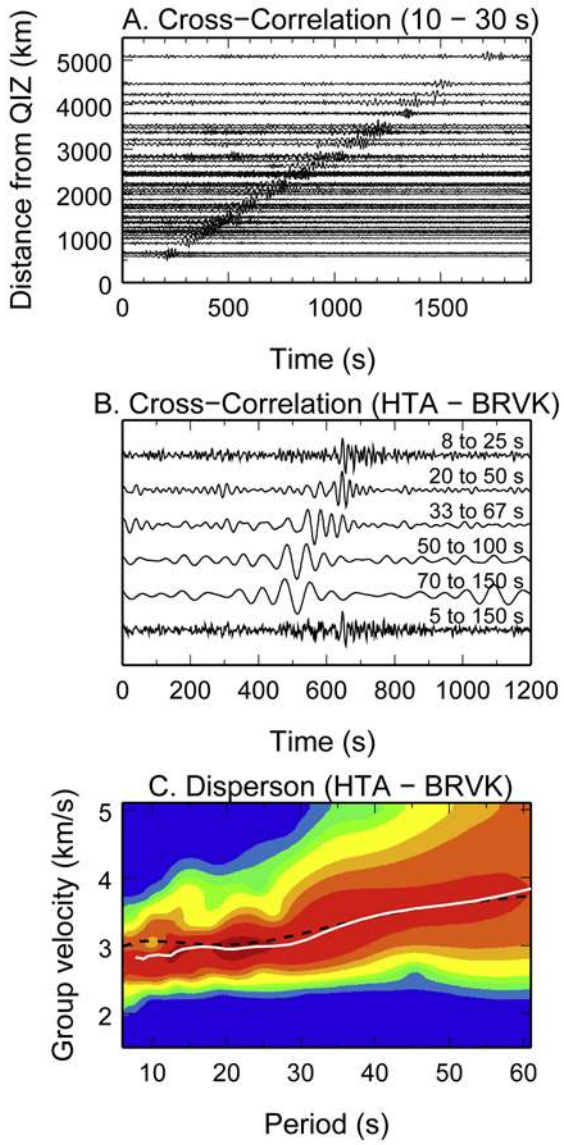

Figure 2. Example of Rayleigh wave EGFs and dispersion measurements obtained from ambient noise correlations. (a) Symmetric component of the correlations between station QIZ (in Hainan Province, China) and other stations. The traces are band pass filtered at relatively short periods (10–30 s). (b) EGFs filtered in different frequency bands. Long-period surface waves are clearly faster than short-period ones. The path is between HTA (bordering Tarim in the south) and BRVK (Borovoye, Kazakhstan). (c) Frequency-time analysis [*Ritzwoller and Levshin*, 1998] used to retrieve Rayleigh wave group velocity dispersion curve (white) for the HTA-BRVK path. The black dashed curve is the prediction from the 3-D global shear velocity model of *Shapiro and Ritzwoller* [2002], which is used for phase-matched filtering in the data analysis and for comparison with measurements.

over 1.5 yearlong time series, is merely a bookkeeping device. The correlation function is often asymmetric with respect to the positive and the negative delays because of non-uniform distribution of noise sources. We use the symmetric component of the correlation as the EGF by averaging the causal and acausal parts of the correlation.

[7] If the signal-to-noise ratio (SNR) is sufficiently large, Rayleigh wave group speeds are then measured using a frequency-time analysis [*Ritzwoller and Levshin*, 1998]. Finally, the inter-station dispersion measurements are used to invert for the Rayleigh wave group velocity maps, in exactly the same way as earthquake-based measurements.

3. Results

[8] For most of the station pairs, we are able to retrieve good Rayleigh wave signals from the ambient noise correlations. Figure 2 shows typical examples of EGFs and group velocity measurements of Rayleigh waves retrieved from ambient noise correlations. The cross correlations show strong arrivals at different settings (near the coast or well into the continental interior) and at both relatively low frequencies (20–50 s) and high frequencies (5–20 s). The EGFs can be retrieved over the entire region (at distances of over 5000 km) (Figure 2a).

[9] We measured group velocity dispersion curves (Figure 2c) for station pairs with Rayleigh wave SNR > 10. The SNR is defined as the ratio of the peak amplitude of the Rayleigh wave to the root-mean square value of the background. The measurement is very stable. Clear dispersion can be commonly observed directly from the EGFs (Figure 2b). We found that the group velocity measurements can extend to periods of 10 s or shorter even for station pairs that are separated over thousands of kilometers. The group velocities of the HTA-BRVK path (Figures 2b and 2c), which samples the Tarim Basin, agree with a global 3-D earthquake-based model [*Shapiro and Ritzwoller*, 2002] at longer periods but differ significantly at short periods (below 30 s). The slow group velocities at short periods are caused by the thick sediments of the Tarim Basin (see discussion below).

[10] We have obtained dispersion measurements with SNR > 10 for periods 8 s to 70 s (Figure 3a). The best observed frequency band is 10 to 30 s with over 1000 measurements at each period or a

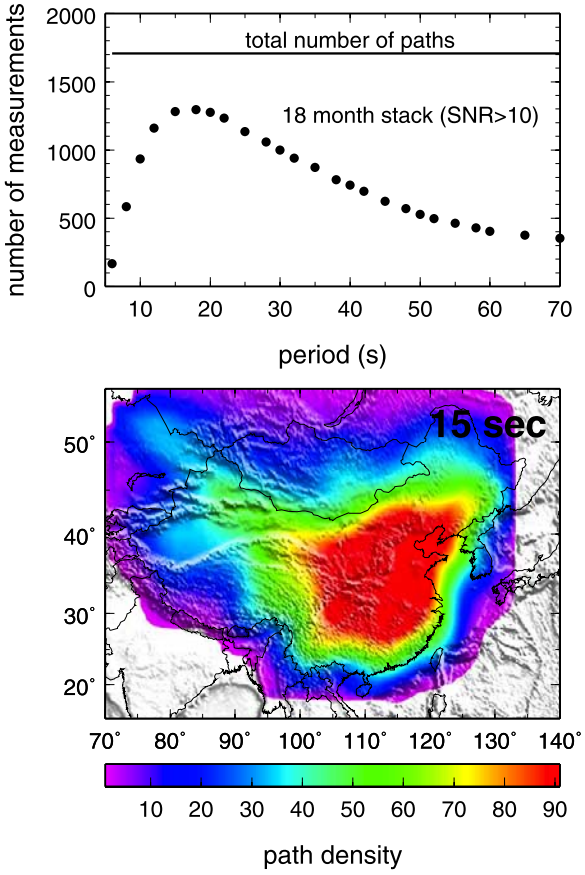

Figure 3. (top) Distribution of dispersion measurements for different periods and (bottom) ray density map for the period of 15 s. (top) The total number of paths takes into account data availability for pairing up stations. (bottom) The ray density is the number of rays inside 1 degree by 1 degree cell. The rays are station pairs for which dispersion measurements have been obtained. The ray coverage is best for periods 10 to 30 s. Coverages for shorter or longer periods deteriorate, but the spatial coverage patterns remain similar.

retrieval rate of 50 to 80% of all the possible pairs. The raypaths cover almost the entire continental China (Figure 3b). However, the coverage is much better in the eastern half of the country, because of the denser station distribution there than in the western part.

[11] The ray coverage of our dispersion measurements is sufficient for us to invert for Rayleigh wave group velocity maps at periods from 8 s to 60 s (Figure 4). The results show remarkable features that correlate with large-scale geological structures of China. Major basins are well delineated with low velocities at short periods (8 to 20 s), including Bohai-Wan Basin (North China Basin), Sichuan Basin, Qaidam Basin, and Tarim Basin. The stable Yangtz Craton also shows up well with high velocities. At longer periods (25–50 s), the group velocity maps display striking bimodal distribution with high velocity in the east and low velocity in the west, which corresponds very well with the thinner crust in the east and much thicker crust in the west [e.g., *Liang et al.*, 2004]. The NNE-SSW trending boundary between fast and slow velocities (around longitude 108°E) coincides with the sharp topographic change and with the well-known Gravity Lineation.

[12] A side-by-side comparison between a short period group velocity map and sediment thickness or between an intermediate period map and crustal thickness is presented in Figure 5. The correlations are quite striking if we compare the group velocities along a certain profile of interest (Figure 6). The selected profile along latitude of about 39°N passes through three major basins: Tarim, Ordos, and Bohai-Wan (Figure 1). The thick sediments in these basins [*Laske and Masters*, 1997] correlate well with slow velocities at periods from 10 to 20 s (Figure 6a). The general trend of decreasing crustal thickness from west to east is well represented by increasing group velocities around 30 s (Figure 6b). However, the group velocity map displays more structure than the smooth crustal thickness curve from the global reference model (CRUST 2.0) (http://mahi.ucsd.edu/Gabi/rem.html), suggesting a more complex Moho. At period 50 s, the trend is no longer observable as the surface waves sample deeper into the mantle.

4. Conclusion and Discussion

[13] Using correlations of 18 months of continuous data from CNSN and global seismic stations, we retrieve Rayleigh wave empirical Green functions (EGFs) over a broad frequency band across China and surroundings. Group velocity dispersion measurements are obtained for periods of 8 to 70 s. The best observed frequency band is 10 to 30 s with a retrieval rate of 50 to 80% of the station-pairs. We have constructed Rayleigh wave group velocity maps of China from 8 to 60 s. The tomographic maps show remarkable correlations with the major tectonic features of China, in particular, the major sedimentary basins and crustal thickness. With the rapid growth of digital seismic stations in China, we are hopeful to see much improved tomographic images of the structures of the region in the near future.

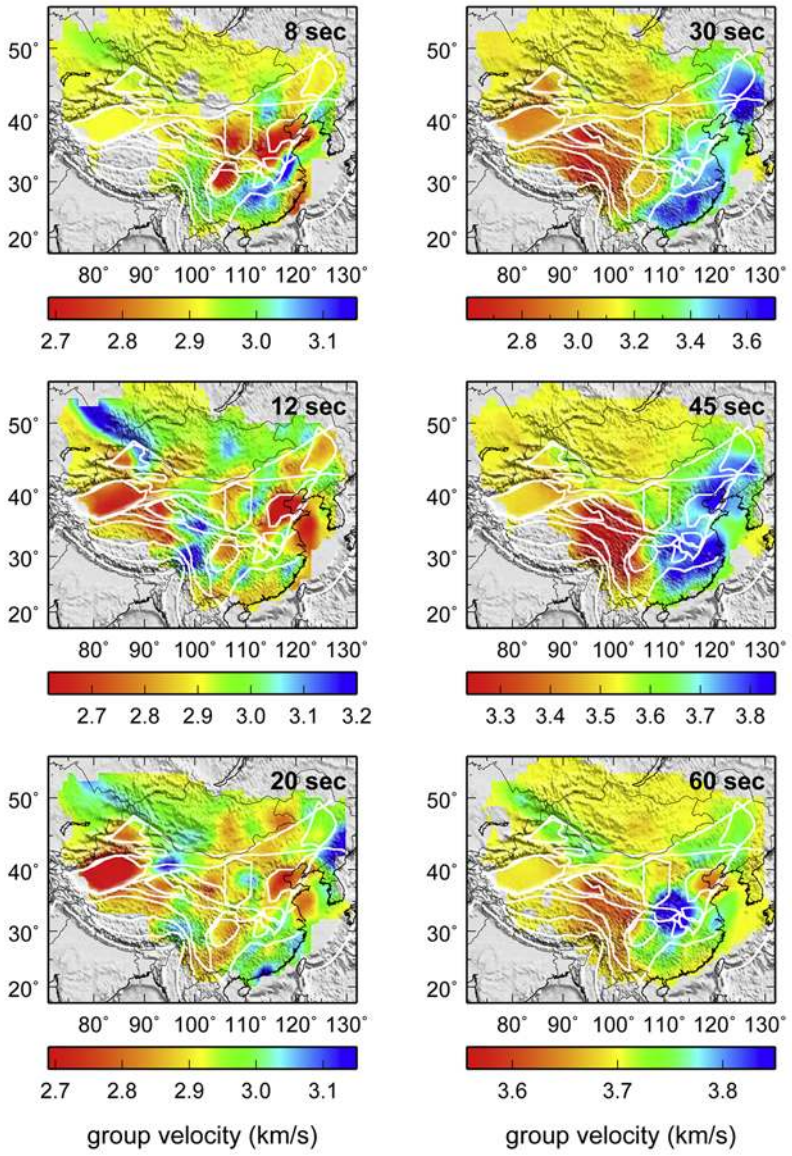

Figure 4. Maps of Rayleigh wave group velocities at periods of 8, 12, 20, 30, 45, and 60 s. Note the color scale for each period is selected so that the scale represents the range of the values with the average value in the middle of the color bar (between yellow and green). The ranges of the values for different periods are different. Plotted in the background are major block boundaries and basin outlines (Figure 1).

[14] Comparison of the tomographic maps with the geological features discussed above provides an important initial validation of the ambient noise tomography (ANT) methodology; i.e., the method provides models of group wave speeds that are consistent with well-known geological features and other geophysical observations. Furthermore, the complete repeatability of the ANT method makes it possible to validate directly the methodology and to evaluate the uncertainties of the dispersion measurements. Several methods have been proposed in this regard. (1) Direct verification: Comparing the EGF with the surface wave generated by an earthquake along the same path [e.g., *Shapiro et al.*, 2005; *Bensen et al.*, 2007]. (2) Comparing the EGF obtained from ambient noise and that from seismic coda [*Yao et al.*, 2006]. (3) Temporal stability: Comparing the EGFs from the data observed at different time periods (e.g., different months) [*Shapiro et al.*, 2005; *Yao et al.*, 2006; *Bensen et al.*, 2007]. Furthermore, because the principal ambient noise sources are believed to come from the oceans [e.g., *Yang and Ritzwoller*, 2008], which are seasonal, the consistency of the correlations from different seasons gives a measure of the stability and error of the EGFs [*Bensen et al.*,

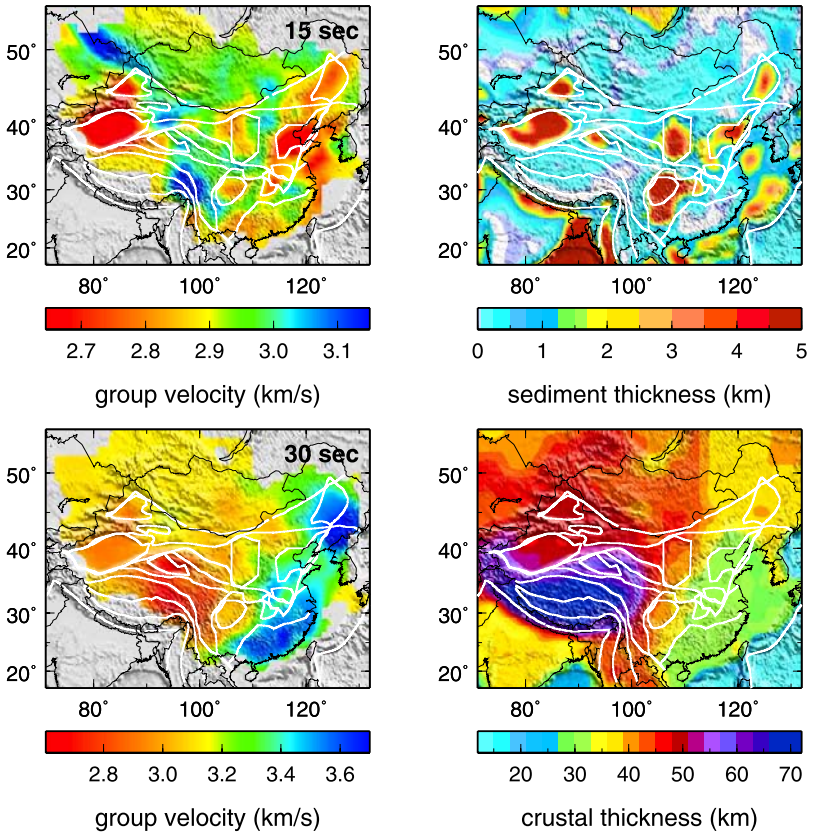

Figure 5. Comparison of group velocities with (top) sediment thickness and (bottom) crustal thickness. Plotted in the background are major block boundaries and basin outlines (Figure 1). (top) The group velocity map (left) is for 15 s Rayleigh waves. The major basins (including Tarim, Junggar, Qadaim, Sichuan, Bohai Wan, and Songliang as well as the southern North China and Jianghang basins in the east central region) are well delineated by slow velocities. See Figure 1 for the locations of the basins. (bottom) The group velocity map is for 30 s Rayleigh waves. The major trend of crust thickening from the east to west (right) is well represented by the velocity decreases from east to west (left).

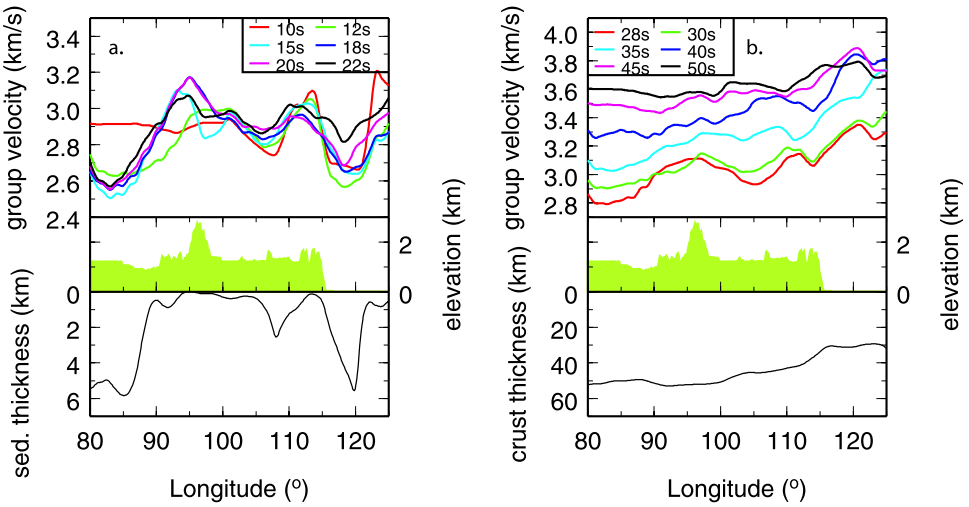

Figure 6. Rayleigh wave group velocities are compared with (a) sediment thickness and (b) crustal thickness along a selected path. The selected path is along the great circle path between (38°N, 80°E) and (38°N, 125°E), passing through three major basins (Tarim, Ordos, and Bohai Wan) (Figure 1). Plotted at the top are velocities (a) for shorter periods and (b) for longer periods. Plotted at the bottom are (a) sediment thickness and (b) crustal thickness. In the middle are surface elevations.

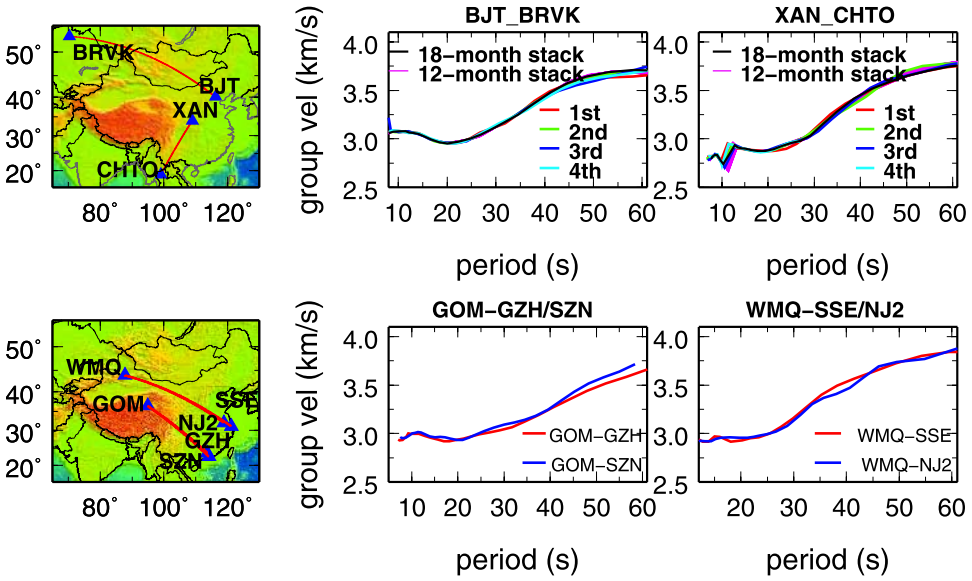

Figure 7. (top) Temporal and (bottom) spatial consistency of dispersion measurements. (top) Comparison of dispersion curves from different time windows. We select two pairs, BJT-BRVK along an east-west path and XAN-CHTO along a north-south path. For each pair, we calculate two sets of EGFs. For each calculation of the EGF, a total of 12 months of data are used. The 18-month stack (including all the data we collected) is plotted for comparison. One set uses seasonal data (red, green, blue, and cyan), i.e., data from the same season over a period of 4 years. The other set uses 12 months of data with a sliding time window of 10 d (total of 19 curves, all in magenta). (bottom) Comparison of dispersion curves between a far-away station and two close stations. We select two pathways, one from GOM to GZH/SZN (distance about 2400 km) and the other from WMQ to SSE/NJ2 (distance about 3100 km). The distance between GZH and SZN is about 133 km, and that between SSE and NJ2 is 245 km.

2007]. (4) Spatial consistency: Comparing the EGFs for station-pairs along similar paths [*Bensen et al.*, 2007]. The EGFs between a far-away station to two or more stations that are close to one another should be similar as the paths sample similar structure.

[15] We have examined temporal and spatial consistency of our dispersion measurements and found that they are very consistent whenever the SNRs of the EGFs are high. Some examples are shown in Figure 7. The temporal comparisons include a station pair with an east-west path (BJT-BRVK) and another pair with a north-south path (XAN-CHTO) (Figure 7, top). We construct 23 dispersion curves using 12-months of data with different sliding windows or using 12-months of data over different seasons. For either pair, we find the standard deviation of these curves to be less than 2% for all periods and the standard deviation of the mean to be less than 0.5%. The spatial comparisons include two pathways (Figure 7, bottom), from GOM to GZH/SZN and from WMQ to SSE/NJ2. The group velocities between WMQ and SSE are quite similar to those between WMQ and NJ2 at all the observed periods (10 to 60 s). The group velocities between GOM-GZH and GOM-SZN are also similar at periods less than 40 s. At periods greater than 40 s, they are somewhat different but are within the uncertainties as indicted in the temporal plots (Figure 7, top). A future effort will be to quantify systematically the uncertainties of the dispersion measurements and the velocity tomography using repeated measurements and repeated tomography.

Acknowledgments

[16] The CNSN waveform data were provided by China Earthquake Network Center, and other station data were obtained from IRIS DMC. We thank reviews from two anonymous reviewers. One review was particularly constructive and detailed, which helped improve the paper greatly. The figures were made using GMT software [*Wessel and Smith*, 1998]. The groups at UIUC and CU acknowledge support from Federal grants AFRL FA8718–07-C-0006, NSF EAR-0330749 (UIUC), and NSF EAR-0337622 (CU).

References

Bensen, G., et al. (2007), Processing seismic ambient noise data to obtain reliable broad-band surface wave dispersion measurements, *Geophys. J. Int.*, *169*(3), 1239–1260, doi:10.1111/j.1365-246X.2007.03374.x.

Bensen, G. D., M. H. Ritzwoller, and N. M. Shapiro (2008), Broadband ambient noise surface wave tomography across the United Stated, *J. Geophys. Res.*, *113*, B05306, doi:10.1029/2007JB005248.

Campillo, M. (2006), Phase and correlation in random seismic fields and the reconstruction of the Green function, *Pure Appl. Geophys.*, *163*, 475–502, doi:10.1007/s00024-005-0032-8.

Campillo, M., and A. Paul (2003), Long-range correlations in the diffuse seismic coda, *Science*, *299*, 547–549, doi:10.1126/science.1078551.

Curtis, A., et al. (1998), Eurasian fundamental mode surface wave phase velocities and their relationship with tectonic structures, *J. Geophys. Res.*, *103*, 26,919–26,947, doi:10.1029/98JB00903.

Huang, Z. X., et al. (2003), Rayleigh wave tomography of China and adjacent regions, *J. Geophys. Res.*, *108*(B2), 2073, doi:10.1029/2001JB001696.

Kang, T.-S., and J. S. Shin (2006), Surface-wave tomography from ambient seismic noise of accelerograph networks in southern Korea, *Geophys. Res. Lett.*, *33*, L17303, doi:10.1029/2006GL027044.

Laske, G., and G. Masters (1997), A global digital map of sediment thickness, *Eos Trans. AGU*, *78*(46), Fall Meet. Suppl., F483.

Lebedev, S., and G. Nolet (2003), Upper mantle beneath Southeast Asia from S velocity tomography, *J. Geophys. Res.*, *108*(B1), 2048, doi:10.1029/2000JB000073.

Liang, C., and C. A. Langston (2008), Ambient seismic noise tomography and structure of eastern North America, *J. Geophys. Res.*, *113*, B03309, doi:10.1029/2007JB005350.

Liang, C., X. Song, and J. Huang (2004), Tomographic inversion of Pn travel times in China, *J. Geophys. Res.*, *109*, B11304, doi:10.1029/2003JB002789.

Lin, F., M. P. Moschetti, and M. H. Ritzwoller (2008), Surface wave tomography of the western United States from ambient seismic noise: Rayleigh and Love wave phase velocity maps, *Geophys. J. Int.*, *173*(1), 281–298, doi:10.1111/j1365-246X.2008.03720.x.

Lobkis, O. I., and R. L. Weaver (2001), On the emergence of the Greens function in the correlations of a diffuse field, *J. Acoust. Soc. Am.*, *110*, 3011–3017, doi:10.1121/1.1417528.

Paul, A., M. Campillo, L. Margerin, E. Larose, and A. Derode (2005), Empirical synthesis of time-asymmetrical Green functions from the correlation of coda waves, *J. Geophys. Res.*, *110*, B08302, doi:10.1029/2004JB003521.

Ritzwoller, M. H., and A. L. Levshin (1998), Eurasian surface wave tomography: Group velocities, *J. Geophys. Res.*, *103*, 4839–4878, doi:10.1029/97JB02622.

Sabra, K. G., P. Gerstoft, P. Roux, W. A. Kuperman, and M. C. Fehler (2005a), Extracting time domain Green's function estimates from ambient seismic noise, *Geophys. Res. Lett.*, *32*, L03310, doi:10.1029/2004GL021862.

Sabra, K. G., P. Gerstoft, P. Roux, W. A. Kuperman, and M. C. Fehler (2005b), Surface wave tomography from microseisms in Southern California, *Geophys. Res. Lett.*, *32*, L14311, doi:10.1029/2005GL023155.

Shapiro, N. M., and M. Campillo (2004), Emergence of broadband Rayleigh waves from correlations of the ambient seismic noise, *Geophys. Res. Lett.*, *31*, L07614, doi:10.1029/2004GL019491.

Shapiro, N. M., and M. H. Ritzwoller (2002), Monte-Carlo inversion for a global shear velocity model of the crust and upper mantle, *Geophys. J. Int.*, *151*, 88–105, doi:10.1046/j.1365-246X.2002.01742.x.

Shapiro, N. M., M. Campillo, L. Stehly, and M. H. Ritzwoller (2005), High resolution surface wave tomography from ambient seismic noise, *Science*, *307*(5715), 1615–1618, doi:10.1126/science.1108339.

Villaseñor, A., Y. Yang, M. H. Ritzwoller, and J. Gallart (2007), Ambient noise surface wave tomography of the Iberian Peninsula: Implications for shallow seismic structure, *Geophys. Res. Lett.*, *34*, L11304, doi:10.1029/2007GL030164.

Weaver, R. L. (2005), Information from seismic noise, *Science*, *307*, 1568–1569, doi:10.1126/science.1109834.

Wu, F. T., A. L. Levshin, and V. M. Kozhevnikov (1997), Rayleigh wave group velocity tomography of Siberia, China and the vicinity, *Pure Appl. Geophys.*, *149*, 447–473, doi:10.1007/s000240050035.

Xu, G. M., et al. (2000), The 3-D structure of shear waves in the crust and mantle of east continental China inverted by Rayleigh wave data, *Chin. J. Geophys.*, *43*(3), 395–406.

Yang, Y., and M. H. Ritzwoller (2008), Characteristics of ambient seismic noise as a source for surface wave tomography, *Geochem. Geophys. Geosyst.*, *9*, Q02008, doi:10.1029/2007GC001814.

Yang, Y. J., M. H. Ritzwoller, A. L. Levshin, and N. M. Shapiro (2007), Ambient noise Rayleigh wave tomography across Europe, *Geophys. J. Int.*, *168*, 259–274, doi:10.1111/j.1365-246X.2006.03203.x.

Yao, H. J., et al. (2005), Mantle structure from inter-station Rayleigh wave dispersion and its tectonic implication in western China and neighboring regions, *Phys. Earth Planet. Inter.*, *148*(1), 39–54, doi:10.1016/j.pepi.2004.08.006.

Yao, H. J., R. D. van der Hilst, and M. V. de Hoop (2006), Surface-wave array tomography in SE Tibet from ambient noise and two-station analysis - I. Phase velocity maps, *Geophys. J. Int.*, *166*(2), 732–744, doi:10.1111/j.1365-246X.2006.03028.x.

Zhang, Y. S., and T. Lay (1996), Global surface wave phase velocity variations, *J. Geophys. Res.*, *101*, 8415–8436, doi:10.1029/96JB00167.

Zhu, J. S., et al. (2002), High resolution surface wave tomography in East Asia and West Pacific marginal seas, *Chin. J. Geophys.*, *45*(5), 679–698.